https://doi.org/10.5194/wes-2024-90
Preprint. Discussion started: 20 August 2024

WIND ENERGY SCIENCE DISCUSSIONS

Flight guidance concept for the launching and landing phase of a flying wing used in an airborne wind energy system

Dominik Felix Duda , Hendrik Fuest , Tobias Islam , and Dieter Moormann

Institute of Flight System Dynamics, RWTH Aachen University
Wüllnerstraße 7
52062 Aachen, Germany

Correspondence: Dominik Felix Duda (duda@fsd.rwth-aachen.de)

Abstract. Airborne wind energy is an emerging technology that utilizes tethered airborne systems in wind fields to harvest energy. The employment of flying wings as airborne systems holds considerable promise concerning system performance, given their favorable aerodynamic characteristics. Moreover, when designed as motorized tailsitter, they can provide vertical takeoff and landing capabilities. However, the processes of launching, defined as the transition from takeoff to energy-harvesting flight, and landing, defined as the transition back, present considerable challenges for such flying wing AWES. To ensure the safe operation of the flying wing, it is essential to consider the controllability at varying wind speeds and the limitations imposed by the tether. To address this, a suitable guidance concept for the launching and landing phases of the aforementioned flying wing AWES has been devised. The concept is subjected to analysis taken into account specific system parameters, including turning radius, operating height, and wind speed. In light of these considerations, a flight regime can be identified. This is considered in the design of a guidance controller, which represents the top level of a cascaded flight controller. The lower levels of the controller comprise a translational controller and a rotational controller. The performance of the overall controller is demonstrated through a simulation of a representative wind field and corresponding system parameters. The results indicate that the control concept successfully facilitates the desired launching and landing in simulations. Future research may build upon the developed guidance and focus on identifying additional and more arbitrary flight paths for launching and landing.

1 Introduction

The development of new technologies to harvest renewable energy sources, such as wind energy, has become increasingly important. In addition to the established wind turbines, airborne wind energy (AWE) has emerged as a new technology. Configured as a ground power generation airborne wind energy system (ground-gen AWES), it consists of at least one airborne system that flies in the wind while tethered to a winch on the ground. Figure 1 illustrates the working principles of such ground-gen AWES. For this configuration, the energy-harvesting flight comprises two alternating phases: power generation and recovery. During the energy generation phase, aerodynamic forces build up on the wing of the airborne system. In this wing-borne operation, the aerodynamic forces exerted on the wing exceed the force of gravity, allowing the system to remain airborne and pull on the tether. At the winch, this pull causes the tether to unwind from a drum, driving an electric generator. When the airborne system reaches the maximum allowable tether length, it exits the generation phase and enters the recovery phase. During this

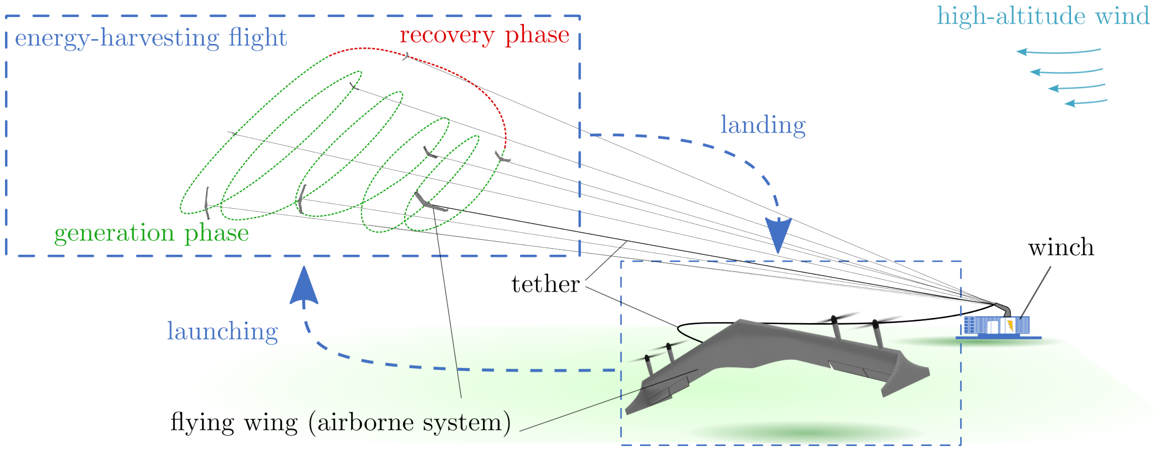

Figure 1. General working principles and problem formulation of launching and landing for a flying wing AWES in ground-gen configuration.

phase, the airborne system returns to its initial position while the winch retracts the tether. After that, the generation phase commences anew. Alternatively to the ground-gen AWES, the flying airborne system can perform power generation directly. For such flying power generation (fly-gen) AWES, specialized turbines are employed along the wing to generate electricity on board. Tethers with integrated electric cables are used to transmit the energy to the ground (Ahrens et al., 2013). Many approaches to guidance and control of AWES can be found in the literature. However, most emphasize the energy-harvesting flight, not the launching or landing (Sieberling, 2013; Fagiano et al., 2014; Rapp, 2019). For this reason, this paper addresses these two operational phases for a specific flying wing AWES.

Generally, for both ground-gen and fly-gen AWES configurations, the airspeed at the airborne system must be sufficient to generate lift to achieve wing-borne flight. Depending on aerodynamic performance and weight, the AWES requires different airspeeds or cut-in ambient wind speeds, meaning the minimum speed of the prevailing wind that will generate enough lift to keep the tethered airborne system in the air so that it can eventually transition to energy-harvesting flight. For example, lightweight soft-wing kites, such as the PN-14 from SkySails Power GmbH shown in Fig. 2a, require a deficient cut-in ambient wind speed of only 5-6 m/s to sufficiently inflate the kite and provide enough supporting lift (AWEurope, 2024). However, as Loyd (1980) has demonstrated, the performance of an AWES is strongly contingent upon the lift-to-drag ratio of the airborne system. Consequently, minimizing the airborne system's drag and maximizing its glide ratio represent pivotal design considerations. As soft-wing kites are prone to exhibiting markedly inferior aerodynamic performance in comparison to fixed-wing airborne systems, a design drive towards these fixed-wing AWES has taken place in recent years. However, implementing a fixed-wing airborne system design entails an increased mass, which in turn results in higher cut-in ambient winds. The company Mozaero (formerly Ampyx Power) is developing such fixed-wing AWES in ground-gen configuration. Their system shown in Fig. 2b has a wingspan of 12 m and is designed for a power output of 150 kW. To achieve sufficient airspeed, their airborne system accelerates on a runway, enabling launching similarly to conventional aircraft. However, if the goal is to design AWES as a flexible installed energy system requiring minimal ground space, it necessitates omitting the runway. An alternative solution is a catapult-like mechanism, which addresses the issue of insufficient airspeed during launching and landing while providing the needed flexibility. This additional launching and landing aid system accelerates the airborne system to achieve the required airspeed for wing-borne flight even when the actual cut-in ambient wind speed is relatively low, providing greater flexibility and an extended operating range for fixed-wing AWES. In the field of AWE, EnerKite GmbH has been a pioneer in the development of fixed-wing AWES. They have implemented a swiveling mast, shown in Fig. 2c, to accelerate the airborne system, allowing it to achieve sufficient airspeed, generate lift, and get airborne. In addition to employing a fixed-wing configuration, Enerkite designs its airborne system as a flying wing. This configuration reduces the airborne system to a single wing without a tail, which allows for an increase in its aerodynamic performance and thus can potentially improve the overall AWES performance (Martinez-Val, 2007; Liang et al., 2017; Wohlfahrt and Nickel, 1990).

Conversely, the objective is to design a fixed-wing AWES but eliminate a rotating launch catapult mechanism and enable the airborne system to operate more independently. In that case, the airborne system must have its propulsion units. When configured as a tailsitter, the motorization enables the airborne system to perform propeller-borne vertical takeoff and landing (VTOL) in an upright position with the nose pointing upward (Liang et al., 2017; Ritz and D'Andrea, 2017). Based on this propeller-borne operation, referred to as prop-borne, the airborne system can adjust the thrust direction to accelerate until the airspeed around the wing generates lift. As airspeed and lift continue to increase, the airborne system transitions to wing-borne flight. Full wing-borne flight is achieved when the generated lift balances the gravitational load and all other loading forces. In the field of fly-gen AWES, the former company Makani Technologies LLC has historically held a prominent position. Their M600, shown in Fig. 2d, features a tailsitter-like design. However, the M600 is not designed as a flying wing, as it has a tail attached to the wing. It was the subject of extensive testing, even in offshore conditions, and was the largest ever built AWES until today. After the dissolution of the company in 2020, all technical studies were made publicly available online (Makani Technologies LLC, 2020a). As detailed in the technical report from Makani Technologies LLC (2020b), the M600 was anticipated to have a cut-in ambient wind speed of approximately 5-6 m/s, comparable to the operational flexibility of the Skysails PN-14. In order to stabilize the longitudinal motion of the M600 while facing downwind, differential thrust was used for vertical operation, allowing the system to take off and land with the tether stretched. During this vertical flight phase, the thrust from the airborne system actively controlled the tether tension. From there, the tether was unwound to reach the desired tether length for energy-harvesting flight while the airborne system flew downwind. Subsequently, it accelerated upward to enter crosswind flight with a circular flight path. For the transition back to the ground, the M600 decelerated when the system was in the upward motion of the circular path, leaving the crosswind flight. It then hovered back to the ground station. In recent years, the company KiteKRAFT GmbH, shown in Fig. 2e with their current AWES prototype, has followed in Makani's footsteps and developed a tailsitter fly-gen AWES with a very similar concept.

https://doi.org/10.5194/wes-2024-90
Preprint. Discussion started: 20 August 2024

(a) SkySails Power GmbH (b) Mozaero (c) EnerKite GmbH

(d) Makani Technologies LLC (e) KiteKRAFT GmbH (f) Kitemill (g) TwingTec

Figure 2. Representative AWES implemented by the industry.

Although the design approaches of these two companies provide the airborne system with a certain level of control authority, it still requires a landing platform with a unique mechanical support structure to mount it on the ground. Alternatively, companies such as Kitemill and TwingTec, shown in Fig.s 2f and 2g, have developed airborne systems configured as quad-plane also providing VTOL capabilities and requiring only a smooth platform for takeoff and landing. In addition, the airborne systems can detach from the tether and fly independently of the winch, delivering increased system flexibility. In terms of deployment in an AWE find farm, airborne systems can operate independently to a central maintenance station. For these quad-plane AWES, a multi-copter mode first brings the airborne system downwind (Rapp and Schmehl, 2018). Once the AWES reaches a desired tether length, the airborne system is accelerated by rapid tether retraction controlled by the winch. When it reaches the minimum airspeed for wing-borne operation, the VTOL controller fades out, and guidance for the generation phase is activated. A full technical report can be found in Houle and Luchsinger (2021) for more information on these quad-plane AWES.

In terms of improved overall AWES performance, the combination of a flying wing airborne system, as pursued by EnerKite, with the ability to take off and land independently and propelled, as envisioned by Makani, kiteKRAFT, Kitemill, or TwingTech, is promising. For such a flying wing configuration, propulsion units can be attached to the wing to direct the thrust vector in the longitudinal axis of the airborne system. Considering that the flying wing AWES is designed as a ground-gen AWES, the propulsion units are turned off, and the propellers are retracted during the generation and recovery phases. However, when assuming a fly-gen AWES, these propulsion units can be inverted and used as specialized turbines for the energy-harvesting flight. This paper investigates such a flying wing AWES with VTOL capabilities as illustrated in Fig. 1. It focuses on developing suitable guidance for launching and landing this specific flying wing AWES. The following presents a guidance concept in Section 2. Based on this, the system is analyzed for specific operation parameters and wind speeds to

https://doi.org/10.5194/wes-2024-90
Preprint. Discussion started: 20 August 2024

identify a flight regime (Section 3). This allows for designing a guidance controller in Section 4. In Section 5, results for a model in a loop simulation with the developed controller, a representative wind field, and corresponding operation parameters are presented and discussed. Finally, Section 6 gives this work's conclusion and outlook.

2 Guidance concept

The launching and landing of the flying wing AWES can be divided into a transition from prop- to wing-borne and back, but also into phases of increasing and decreasing the tether load (see Fig. 3). In contrast to the airborne systems designed by Makani or KiteKRAFT, the flying wing tailsitter considered does not incorporate a horizontal stabilizer. Furthermore, in contrast to the quad-plane airborne systems developed by Kitemill and Twingtech, the flying wing does not incorporate propulsion units with an offset to the wing plane that could provide additional pitch motion control with differential thrust. Therefore, the designed configuration of the airborne system as a flying wing, driven by aerodynamic performance for wing-borne flight, results in high sensitivity and limited controllability with respect to airspeed perpendicular to the wing, particularly during vertical flight (Fuest et al., 2021b). In a previous study, Fuest et al. (2021a) examined the impact of the tether during vertical flight. While the tether can be utilized as an additional control mechanism, the direct force control from the airborne system during vertical flight is accompanied by a pronounced minimum-phase characteristic, which presents a significant challenge to this control. This phenomenon was also observed by Makani Technologies LLC (2020b) during a vertical tethered downwind flight. Therefore, controlling the tether force and performing a downwind vertical flight with the flying wing, which has even more critical flight characteristics in this flight phase than Makanis M600, is a highly complex undertaking. An innovative alternative approach, as depicted in Fig. 3, takes into account the sagging of the tether during the transition from vertical prop-borne flight to wing-borne flight, and its subsequent tensioning. This approach offers a significant advantage by allowing the

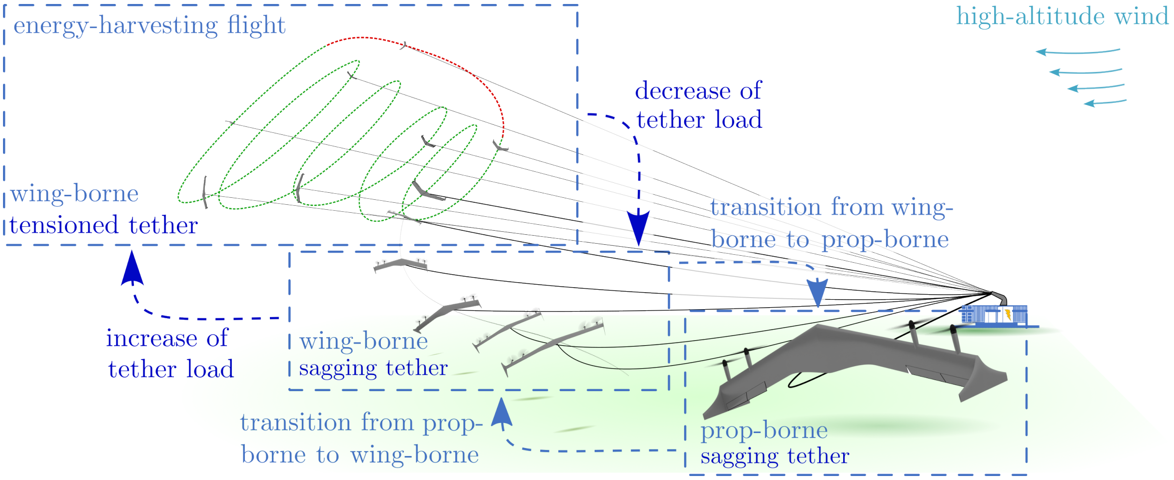

Figure 3. Decomposition of launching and landing of flying wing AWES into partial phases (shown for ground-gen configuration).

tether force control to remain within the airborne system, thereby reducing the associated control complexity. Thus, the winch remains passive in the control scheme, effectively representing the tether's anchor point on the ground. The tensioning of the tether can be achieved during wing-borne flight by increasing the turn radius through the roll motion of the airborne system. As a result, the minimum phase characteristic that arises in vertical flight is no longer present. Nevertheless, when the tether is tensioned, it is important to note that a sudden transition from sagging to stretching can result in force peaks that can lead to critical flight states (Duda et al., 2022; Eijkelhof and Schmehl, 2022). However, as the wing-borne flight for such a flying wing is least sensitive to perturbations, it is desirable to tension the tether in this flight phase only (Fuest et al., 2021b). In order to achieve the sagging of the tether and prevent the unexpected force peaks during the aforementioned transition to wing-borne flight or back to prop-borne flight, it is necessary to maintain a tether length ratio of k greater than one. This ratio is defined as the ratio of the tether length, represented by l_t, and the direct distance from the airborne system to the winch, represented by R_t. Thus, a tether length ratio of $k \geq 1.05$ allows a transition to wing-borne flight and back, without significant disturbance from the material tether tension. However, to guarantee this, it is essential to maintain a minimal position deviation throughout the transition from prop- to wing-borne flight and vice versa. By ensuring that the tether remains sagging throughout these transitions and subsequently considering the stretching of the tether in a wing-borne flight only, the complexity of the control problem is significantly reduced.

In the case of flying wing tailsitters, the transition from prop- to wing-borne flight and vice versa can typically be achieved through a pure pitch transition. This is accomplished through the implementation of control architectures that utilize switching logic to select between a prop- and wing-borne flight controller (Stone et al., 2008; Jung et al., 2013; Hochstenbach et al., 2015; Wang et al., 2015). Nevertheless, the flight regime for a pure pitch transition of a flying wing as airborne system is constrained, particularly at lower airspeeds during vertical flight (Fuest et al., 2021b). The control system's complexity is further augmented when the transition with the tether attached to the airborne system is taken into account. Given that the tether is affixed to the bottom of the airborne system, it is essential to ensure that this side is oriented approximately towards the winch to prevent tether entanglement with the airborne system. Given the abovementioned constraints and the objective of achieving a controllable pure pitch transition, such a maneuver would be restricted to top-directed flight on a hemisphere. As illustrated in Fig. 4, the tethered airborne system performs a continuous pitch motion on this flight path while flying towards the zenith. Consequently, the airborne system must transition to a wing-borne flight upon reaching the zenith. This approach necessitates a single-turn transition, which presents challenges for stepwise field testing. Furthermore, the return transition poses additional conceptual difficulties, depicting the overall complexity of achieving a pure pitch transition with a flying wing in an AWE context. As an alternative, we propose a multi-axial yaw-roll transition on a curved flight path around the winch at a fixed height, as illustrated in Fig. 4. This knife-edge-like maneuver couples lateral and longitudinal motion. When performed on the curved path, the distance to the winch can be held constant, allowing the tether to sag and minimizing its interference. Furthermore, a step-by-step test procedure can be conducted along the curved path, obviating the necessity for a test field of several hundred meters long and spanning a vast area. A simpler representation of this multi-axial transition is also illustrated in Fig. 4 as yaw-roll transition along a straight flight path. In this instance, this straight yaw-roll transition is

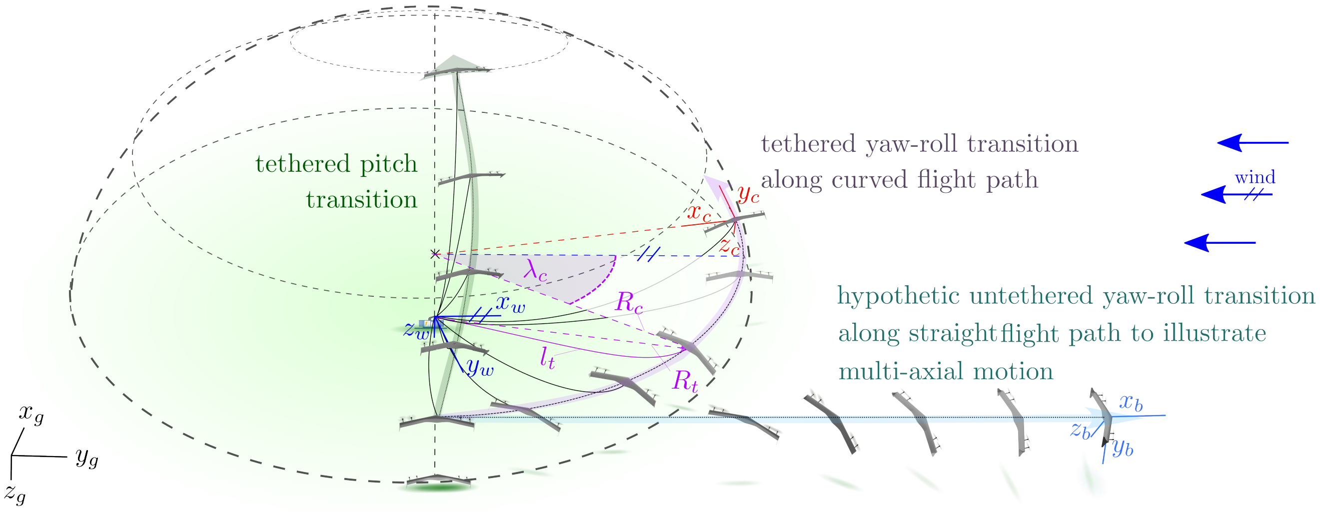

Figure 4. Pitch-transition versus yaw-roll-transition on curved or straight flight path.

presented to clarify the motion of the airborne system. Initially, the airborne system hovers at a defined transition height. At the beginning of this maneuver, the airborne system rotates around the yaw axis to gain speed in the longitudinal direction of the wing (yaw-dominant transition phase). Then, when the airspeed is sufficient, the airborne system rotates about its roll axis (roll dominant transition). The lift force builds up and the airborne system transitions to wing-borne flight. When the transition is performed on a curved path, the distance to the winch can be controlled directly by the airborne system by varying the turning radius. This means that no further winch control of the tether length is required during this operation phase, and the system's overall complexity is reduced. To describe this curved flight path, the cylindrical coordinate system $[\,]_c$ shown in Fig. 4 can be used. There, x_c points to the center of the path curvature, z_c points to the ground, and y_c is tangential to the curved path. In addition, the wind position angle λ_c and the radius of curvature R_c allow to describe the position of the airborne system in the plane of the flight path. In addition, Fig. 4 also illustrates the geodetic $[\,]_g$, body-fixed $[\,]_b$, and wind $[\,]_w$ coordinate systems. This wind coordinate system is defined by x_w pointing upwind. The longitudinal controllability of the flying wing, as analyzed in Fuest et al. (2021b), indicates that aligning the wing plane with the wind direction is essential for ensuring a controlled prop-borne operation at high wind speeds. To guarantee this, the transition is oriented upwards, beginning in a VTOL zone at an approximate wind position angle of $\lambda_c = 90°$ and a fixed radius R_c. This also ensures that sufficient lift is generated in the shortest possible time. In Fuest et al. (2023), we present a preliminary trim analysis of the proposed multi-axial yaw-roll transition along a straight flight path. However, a more comprehensive trim analysis is required when considering centrifugal loads due to a curved flight path and a constant wind field. In the following, we analyze and examine the system for the introduced guidance concept, including trim computations for transitions along curved flight paths with varying wind speeds.

3 System analysis

The following analysis is based on a representative small-scale flying wing demonstrator. A model was developed to identify and analyze controllable flight states at varying wind speeds and operational parameters. In consideration of the proposed guidance concept for launching and landing, this allows for the identification of the flight regime of the flying wing AWES.

3.1 Demonstrator

The airborne system of the AWES under consideration in this study is a small-scale flying wing with a mass of 3.5 kg, depicted in detail in Fig. 5. As shown, this flying wing demonstrator has a wingspan of about 2 m, and is equipped with four propulsion units, two on either side of the wing, situated within the wing plane. Additionally, it is configured with two elevons on each side, positioned within the wake flow of the propulsion units. A detailed description of these controls' general working principle and operational characteristics can be found in Fuest et al. (2021b). As shown in Fig. 1, winglets are attached to the wingtips of the flying wing. These allow this airborne system to stand upright on the ground as a tailsitter and act as vertical stabilizers in wing-borne flight. The wing is designed with the reflexed HS 3.4/12.0B airfoil, which is characterized by a large relative chamber

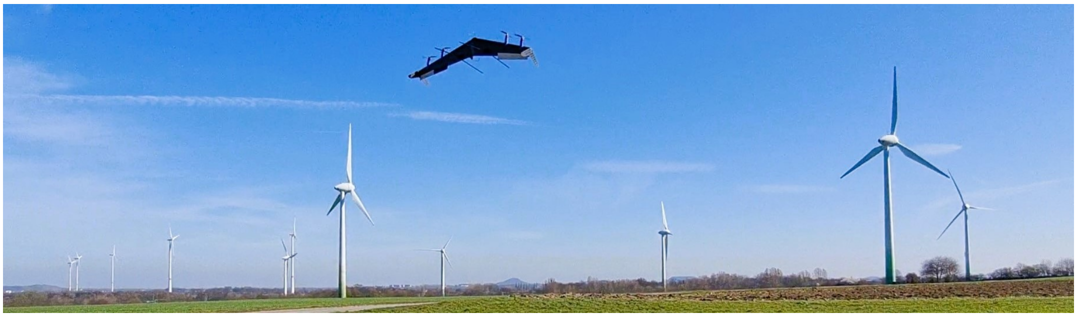

(a) Demonstrator in field test.

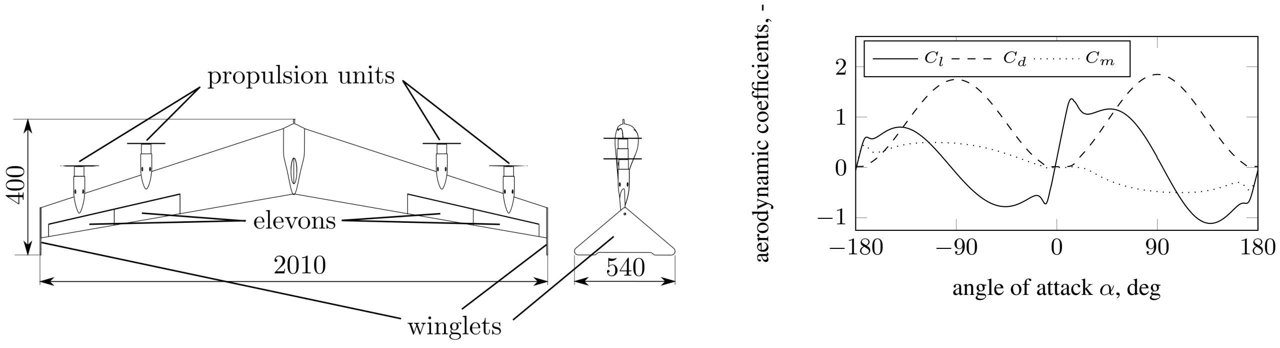

(b) Sketch of demonstrator.

(c) Polar of HS 3.4/12.0B airfoil.

Figure 5. Flying wing demonstrator.

of 3.4 % and relatve thickness of 12.0 % chord length, allowing high lift coefficients in wing-borne flight and very small pitch moments. In contrast to most other flying wing tailsitter investigated by academia in recent years (Li et al., 2018; Tal et al., 2023; Smeur et al., 2020), the aspect ratio of the this flying wing is up to two times higher allowing to reduce the induced drag and improve the potential performance of the AWES. Overall this small-scale demonstrator is intended to be comparable to future demonstrators designed primarily for the energy-harvesting flight phase and thus driven by aerodynamic efficiency. For autonomous operation, the flying wing is equipped with a flight computer and various sensors, such as an inertial measurement unit, a satellite navigation receiver, a wind vane and a servo-controlled pitot tube to estimate flight conditions such as airspeed. In addition, the airborne system is equipped with a load cell to measure the tether force. This load cell is integrated into the tether anchor point of the airborne system, which is located on the underside of the wing and at the center of gravity. The tether is of the Dyneema type, known for its high strength and low weight. It has a diameter of 1 mm and a length between 50 m and 85 m. Regarding the presented guidance concept for launching and landing, the winch of the AWES is considered an anchor point for the tether on the ground. Consequently, the winch is not addressed further in this analysis, and the tether length is treated as fixed throughout the launching and landing process. This simplifies the overall complexity and facilitates field testing.

3.2 Model

The flying wing is modeled as a rigid body with mass m and six degrees of freedom. The translational motion can be described by Eq. (1). Here, $[u\,v\,w]^T$ represents the translational velocity and $[p\,q\,r]^T$ the rotational velocity. In addition to the inertia loads, the thrust is represented by T pointing in body-fixed x_b-direction. The aerodynamic load is represented in the aerodynamic coordinate system $[\,]_a$ by lift L as well as by drag D_x and D_y. This aerodynamic load vector is transformed into the body-fixed system using the coordinate transformation matrix $\mathbf{M}_{[ba]}$. Similarly, gravitational and tether force are transformed into the body-fixed coordinate system using $\mathbf{M}_{[bg]}$ and $\mathbf{M}_{[bt]}$. For the considered tether coordinate system, z_t points in the direction of the winch, x_t points towards the zenith, while y_t results as right-handed coordinate system.

$$\begin{bmatrix}\dot{u}\\ \dot{v}\\ \dot{w}\end{bmatrix}_b = \mathbf{M}_{ba}\begin{bmatrix}\frac{D_x}{m}\\ \frac{D_y}{m}\\ \frac{L}{m}\end{bmatrix}_a + \begin{bmatrix}\frac{T}{m}\\ 0\\ 0\end{bmatrix}_b + \mathbf{M}_{bg}\begin{bmatrix}0\\ 0\\ g\end{bmatrix}_g + \mathbf{M}_{bt}\begin{bmatrix}0\\ 0\\ \frac{F_t}{m}\end{bmatrix}_t + \begin{bmatrix}p\\ q\\ r\end{bmatrix}_b \times \begin{bmatrix}u\\ v\\ w\end{bmatrix}_b \tag{1}$$

The complete angular motion can be described by Eq. (2), where $[\dot{p}\,\dot{q}\,\dot{r}]^T$ are the body-fixed rotational accelerations, I is the inertia tensor, and $[M_x\ M_y\ M_z]^T$ includes all external moments. The external moments are those generated by the thrust, the deflection of the elevons, and the airspeed on the wing. The tether force is assumed to act on the center of mass.

$$\begin{bmatrix}\dot{p}\\ \dot{q}\\ \dot{r}\end{bmatrix} = I^{-1}\left[\begin{bmatrix}M_x\\ M_y\\ M_z\end{bmatrix} - \begin{bmatrix}p\\ q\\ r\end{bmatrix} \times \left(I\cdot\begin{bmatrix}p\\ q\\ r\end{bmatrix}\right)\right] \tag{2}$$

In order to model the aerodynamics of the airborne system, a semi-analytical element based approach according to Hartmann (2017) is applied. In this approach, the wing is decomposed into a discrete number of elements with similar aerodynamic properties, considering the influence of the elevon deflection and the increased airflow on the wing elements in the slipstream of the propellers. The aerodynamic and gravitational forces and moments are summed for all wing elements. In order to appropriately model the tether and keep it suitable for model in the loop simulations, a model similar to Williams (2017) is used. It considers aerodynamic, gravitational, and inertial loads acting on the tether. In the model-in-loop simulation performed to validate the controller, the complete set of equations of motion given in Eq. (1) and Eq. (2) is solved for each simulation time step. As mentioned in the guidance section, this work assumes that the tether length remains constant throughout the considered launching and landing phases. Thus, no winch dynamics are considered.

3.3 Flight regime

In the following, a trim analysis is performed for the presented guidance concept to determine the flight regime. A trim state is generally considered controllable, when all forces and moments are balanced and the controls are within their limits. For such a trim analysis of the launching and landing, we propose a parameterized guidance path divided into multiple phases shown in Fig. 6. To better classify them within the overall AWES operation, the tilted flight path for energy-harvesting crosswind flight is also shown in Fig. 6 between phase (ii) and phase (iii). However, it is not further examined. As illustrated in the figure, all phases have in common that they start at wind position angle $\lambda_c = 90°$ and cover 360°. In the following listing, main characteristics of these four phases are given:

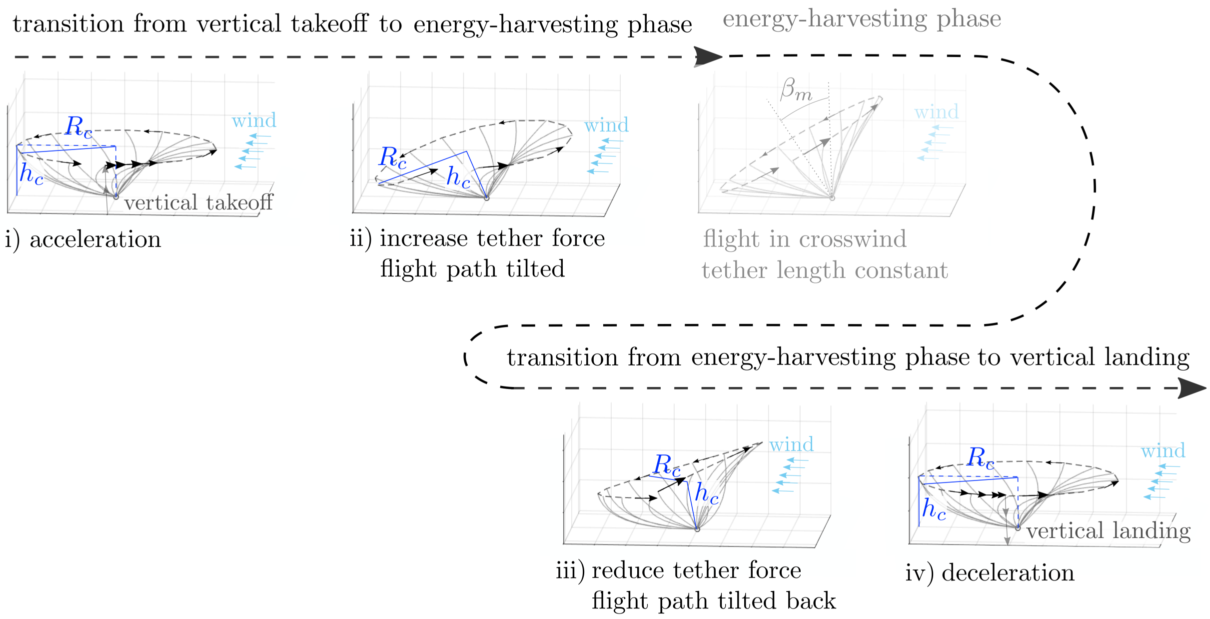

Figure 6. Defined transition phases considered in the trim analysis (radius R_c and height h are given as specific guidance parameters).

https://doi.org/10.5194/wes-2024-90
Preprint. Discussion started: 20 August 2024

i) Curved flight path with turn radius R_c, at fixed height h_c, starting in VTOL zone, and accelerating in upwind direction with 1 m/s^2 up to 16 m/s in airspeed.

ii) Curved flight path with constant airspeed, increasing turn radius until tether is tensioned, and tilting of flight path to mean elevation angle $\beta_m = 10°$.

iii) Curved flight path with constant airspeed, decreasing turn radius until tether is sagging with $k = 1.05$ again, and tilting flight path back to a mean elevation angle of zero.

iv) Curved flight path with turn radius R_c, at fixed height h_c, and deceleration with 1 m/s^2 until VTOL-zone is reached.

Each path is divided into n equally spaced discrete path points for an analysis of these four flight path phases. Based on a prior convergence study, the following analysis is performed for $n = 16$ path points. The aerodynamic velocity $\boldsymbol{V}_a$ at each discrete path point depends on the respective body velocity vector $\boldsymbol{V}_b$ and the wind vector $\boldsymbol{V}_w$ as given in Eq. (3).

$$\boldsymbol{V}_a = \boldsymbol{V}_b - \boldsymbol{V}_w \tag{3}$$

As shown in Fig. 7, we assume that the wind is constant in magnitude and direction. A set of trimmed flight states with associated control settings can be determined based on the aerodynamic velocity at each path point. A trimmed state is given when the equations of motion (Eq. (1) and Eq. (2)) are satisfied. Following the work on the straight yaw-roll transition in Fuest et al. (2023), we seek to identify a set of trimmed flight states for each path point (associated with a specific aerodynamic velocity) by varying the attitude within limits of a predefined grid of different attitude variations. This allows determining

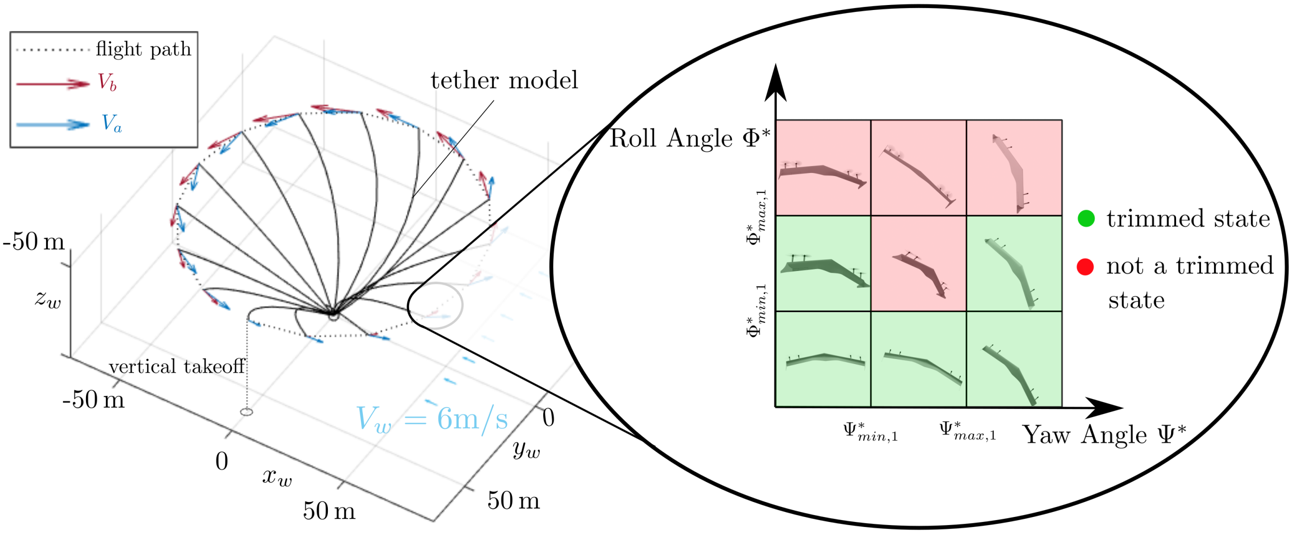

Figure 7. Aerodynamic and body velocities for a curved flight path (phase (i)) as well as attitude variation grid for trim state computation at path point $n = 4$ ($\lambda_c = 68°$).

multiple attitudes that fulfill the trim condition for a considered path point. These trimmed states are marked green, while the others are red in the grid on the right side of Fig. 7. In addition to the general trim conditions, the trimmed flight states must satisfy the following constraints for operation within an AWES:

- The thrust and deflection control of the airborne system must be within the control limits. For the considered small-scale demonstrator, the maximum thrust per engine is set to 18 N and the maximum elevon deflection is set to 30° in each direction.
- Since the airborne system is intended to operate within an AWES, the flight attitude must ensure that the tether can hang freely from the attachment point of the airborne system to the ground station. This condition is considered with a tether operation cone shown in Fig. 8a. This cone is geometrically defined by the distance vector of the tether attachment point at the center of gravity and the position of the inner rotor tips. These points form the boundary of this tether operation cone. Other exposed geometric points such as the winglet edges or the rotor tips of the outer propulsion systems are outside this critical cone. Consequently, it is imperative to ensure that the tether curve at the airborne system remains within the designated operating cone to avert any potential tangling of the tether with the airborne system's components.
- For any trim state of an observed path point, the airborne system must be able to reach at least one new trim state for the following path point. This means that the required rotational rate of the airborne system must be within the dynamic limits of the airborne system. The maximum pitch, roll, and yaw rate for the flying wing demonstrator are set to 30°/s.

With these additional constraints, the trimmed flight states can be computed for each path point. To identify flight states as either prop- or wing-borne, the transition ratio, which is the ratio of the aerodynamic force to the gravitational and tether force, is considered. We define that a transition ratio of 0-0.3 corresponds to prop-borne states, a ratio of 0.3-0.7 to hybrid-borne states, and a ratio of 0.7-1.0 to a wing-borne state (see Fig. 8b). This allows the path points to be associated with the occurring

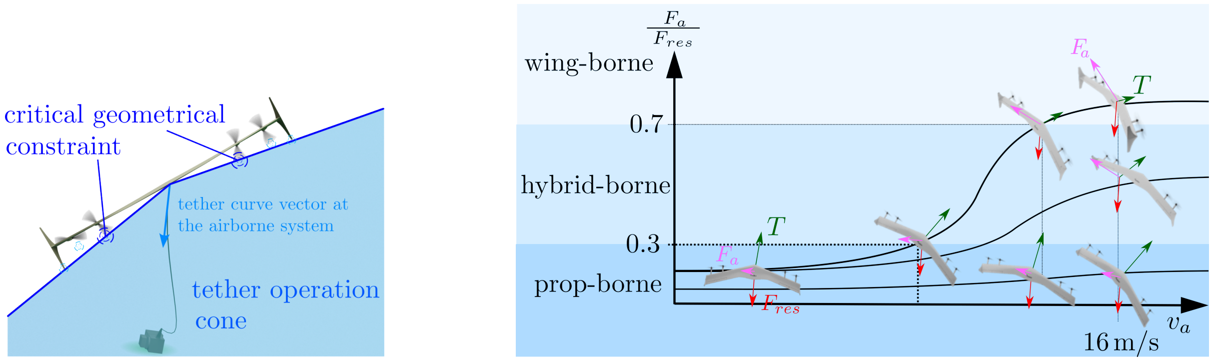

(a) Tether operation cone

(b) Definition of wing- hybrid and thrust borne flight states

Figure 8. Tether operation cone and definition of flight state types.

https://doi.org/10.5194/wes-2024-90
Preprint. Discussion started: 20 August 2024

flight state characteristics: wing-borne, hybrid-borne, prop-borne, a combination of these three, or a non-trimmed state, i.e. an uncontrollable flight state.

Figure. 9 shows the results of two exemplary trim computations corresponding to the transition operation phase (i). Here, the wind speed is assumed to be 6 m/s. For the left configuration (i), the radius R_c is set to 60 m, the height h_c to 50 m, and the tether length ratio to $k = 1.05$. After a vertical start at $\lambda_c = 90°$, the flying wing accelerates upwind in counterclockwise direction. For the first few path points from $\lambda_c = 90°$ to $\lambda_c = 60°$ the emerging airspeed remains below 12 m/s, so that the trimmed flight states have transition ratios below 0.7, meaning that they are prop- or hybrid borne. Moving counterclockwise, the path points from there include states that can be trimmed wing-, hybrid-, and prop-borne. These path points are shown as green circles and represent all three types of flight states. If we consider the same phase for a smaller radius of $R_c = 40$m and at a lower height $h_c = 30$m, as shown in the second configuration (ii) on the right side in Fig. 9, the aerodynamic velocity and the inertial loads along the flight path change. Due to the resulting change in the direction of the tether force at the airborne system, two path points in the range $\lambda_c = 270° - 290°$ cannot be trimmed. In this region, the centrifugal load is higher than average along the flight path as the body speed is increased to maintain a constant airspeed in this downwind region. The reduced turn radius R_c for this configuration (ii) further increases the centrifugal load. Thus, the airborne system must reach an attitude that allows to point the thrust vector more towards the center of the circular flight path to meet the trim condition. The resulting flight states satisfy the general trim condition, but not the extended trim condition considering the additional AWE specific constraints that ensure the tether is within the tether operation cone. Therefore, no controlled states can be found for

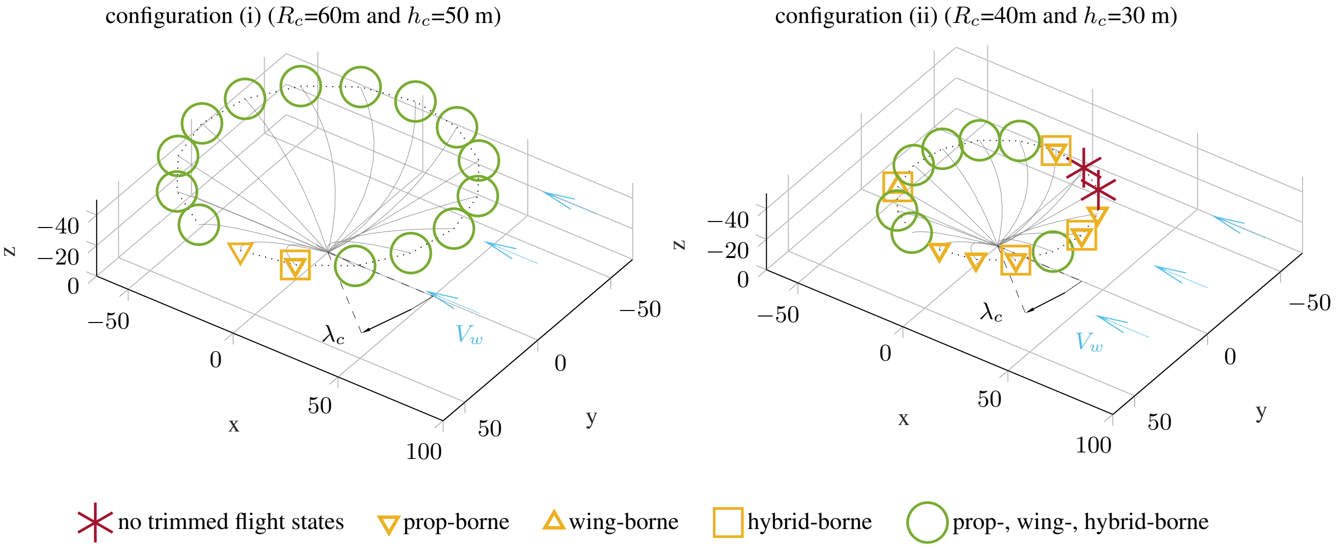

Figure 9. Results from trimm computation for circular flight path with accelerating airspeed up to 16 m/s with an assumed wind speed of 6 m/s. Only the turn radius R_c and transition height h are varied. The tether length ratio is the same ($k = l_{tether}/d = 1.05$)

these two path points. The other yellow path points have flight states that satisfy the extended trim condition. However, the corresponding flight states are only trimmed thrust, hybrid, or wing-borne. This comparison shows the importance of analyzing this flying wing AWES concerning specific operating parameters to ensure the intended operation is controllable. The radius R_c and height h_c for the presented parameterized guidance paths could be identified as critical parameters.

These two guidance parameters are varied for a discrete set of wind speeds ranging from 0 m/s to 14 m/s. The results are plotted in Fig. 10. The parameter combinations that lead to trim computations in which all path points for all four considered phase have trimmed flight states and include the intended flight state are marked in green. This means, for example, that for phase (i), wing-borne flight states can be achieved when the airspeed reaches 16 m/s. On the other hand, for phase(iv), considering the transition back to vertical prop-borne flight before a vertical landing, a trim computation is intended when prop-borne flight states can be reached in the VTOL zone ($\lambda_c = 90°$). All those parameter combinations with path points that cannot be trimmed or do not reach the desired flight state in the considered phase are marked red. The results shown in Fig. 10 overlay the trim computation results corresponding to all four phases. Consistent with the analysis for the two single configurations shown in Fig.9, most of the critical parameter combinations marked red in Fig.10 are due to an increase in centrifugal loads. As it is assumed that for the presented guidance concept the tether must remain sagging during the phase (i) and phase (iv), and that the tether must remain within the tether operating cone, the controllability along the flight path is limited. The area marked green can also be interpreted as the flight regime of this flying wing AWES concerning the considered guidance approach, different wind speeds V_w, and the operating parameters radius R_c and height h_c. Ultimately, this allows to map a measured wind speed to guidance control commands h_{cmd} and $R_{c,cmd}$, ensuring a controllable launching and landing.

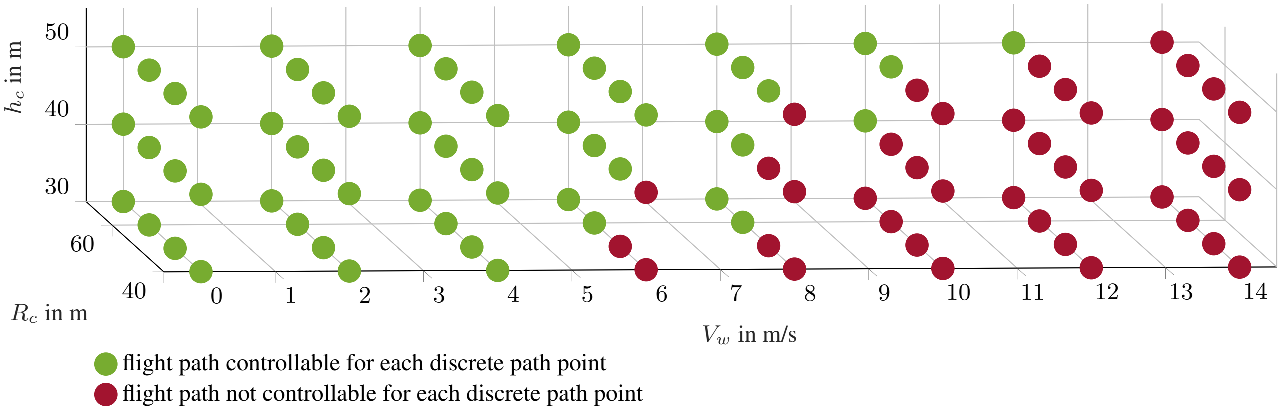

Figure 10. Resulting flight path trim computations for a set of assumed wind speeds V_w and variations of turn radius R_c, and transition height h are distinguished in controllable and not controllable.

4 Controller implementation

This section presents a controller architecture based on the presented guidance concept. As shown in Fig. 11a, the flight controller is cascaded and can be divided into rotational controller, translational controller, and guidance controller. In this paper the focus is placed on the design of the guidance controller. In the following, the architectures of the translational controller and the rotational controller are briefly presented before a detailed description of the guidance controller is given based on the described guidance concept and the determined flight regime.

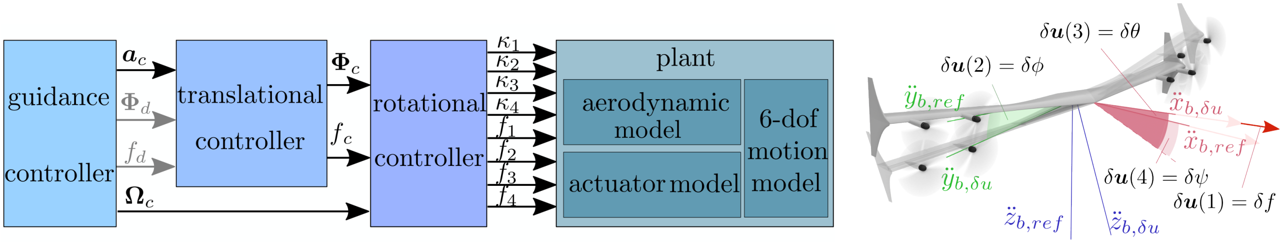

(a) Controller architecture.

(b) Controls of translational INDI controller.

Figure 11. Controller architecture and control vector of the translational INDI controller.

4.1 Underlying rotational and translational controller

As shown in Fig. 11a, the rotational controller on the lowest level of the cascaded controller architecture determines the commands for the four elevons (κ_{1-4}) and the throttle levers for the four propulsion units (f_{1-4}) to control the flight attitude and rotational rate. The prescribed mean thrust (f_c) and attitude commands ($\boldsymbol{\Phi}_c$) serve as input to this rotational controller and are outputs of the superior translational controller. In addition, the guidance controller can directly command a rotational rate ($\boldsymbol{\Omega_c}$), also serving as input for the rotational controller. The entire rotational controller consists of a controller based on rotational incremental nonlinear dynamic inversion (INDI) and a subordinate linear-quadratic regulator (LQR). The LQR provides the required rotational accelerations for the INDI controller. It considers a closed-loop model of the INDI and design weight factors. The general architecture of the INDI controller is presented in Smeur et al. (2016). In the following, only the fundamental concept of the INDI concept is given. Based on Eq. (4), the incremental control $\delta\boldsymbol{u}$ is determined.

$$\delta\boldsymbol{u} = \mathbf{B}^{-1}(\boldsymbol{\nu} - \boldsymbol{x}_f) \tag{4}$$

This incremental control $\delta\boldsymbol{u}$ is computed in each time step as product of the control deviation and the inverse of the effectiveness matrix $\mathbf{B}$. Regarding the rotational INDI, $\mathbf{B}_{rot.}$ considers the effectiveness of the actuators (κ_{1-4} and f_{1-4}), $\boldsymbol{\nu}_{rot.}$ the commanded rotational acceleration from the LQR and $\boldsymbol{x}_{f,rot.}$ the filtered measured rotational acceleration. The incremental control $\delta\boldsymbol{u}_{rot.}$ is accumulated to an estimate of the control $\boldsymbol{u}_{rot}$. Considering a low-pass filter and an actuator model, the control is input to the airborne system actuators. Within this INDI control approach, the design of the effectiveness matrix $\mathbf{B}_{rot.}$ is a core element. The derived matrix entries correspond to the effectiveness of the different controllers concerning the roll, pitch, and yaw motion. See Fuest et al. (2021a) for a detailed description of this rotational controller and validating flight tests.

Like the rotational controller, the translational controller is based on an INDI control approach. As shown in Fig. 11a, the translational controller considers the attitude and the mean throttle in one virtual control vector $\boldsymbol{u}_{trans.} = [\boldsymbol{\Phi}_c, f_c]^T$. The design of the corresponding effectiveness matrix is consistent with our work presented in Müller et al. (2023). However, a peculiarity of the approach used here is that the effectiveness is defined in the body-fixed coordinate systems of the airborne systems. This allows hover prop-borne flight states to avoid singularities in the attitude expression with Euler angles. Based on the INDI control law, only an incremental attitude command is derived, superimposed on the current attitude by a quaternion rotation. For the throttle, the incremental command is summed to an estimated current mean throttle concerning a propulsion model. In contrast to the implemented rotational INDI, the translational controller has another peculiarity. With the four-dimensional controlled variable $\boldsymbol{u}_{trans.} \in \mathrm{I\!R}^4$ and a three-dimensional controlled variable $\boldsymbol{x}_{trans.} \in \mathrm{I\!R}^3$ considering the virtual acceleration commands in all three translational directions, the controlled system is over-determined. Thus, to identify a suitable incremental for the translational controller $\delta\boldsymbol{u}_{trans}$, further weights must be considered. This can be done with an allocation that directly considers the INDI control law, actuator constraints such as a maximum control rate, and weights for the computation of $\delta\boldsymbol{u}_{trans.}$. Within the weights, a desired control vector $\boldsymbol{u}_{d,trans.} \in \mathrm{I\!R}^4$ is considered. Thus, the translational controller needs the virtual translational acceleration commands $\boldsymbol{a}_c$ as control variables and a desired incremental change in mean throttle lever or attitude. Accordingly, if the guidance controller commands a desired positive $\delta\phi_d$ along with an acceleration $\boldsymbol{a}_c$, the translational controller will output a $\delta\boldsymbol{u}_{trans.}$ that initiates a positive roll motion while ensuring that the control law is satisfied.

4.2 Guidance controller

The guidance controller forms the highest cascade of the flight controller. It consists of position and velocity controllers, which control the airborne systems motion concerning the cylindrical coordinate system presented in Fig. 4. In addition to these controllers, a state chart determines the appropriate commands, e.g. the required maximum velocity command during the phase (i). A curve coordination derives the prescribed angular rate to ensure a curve coordinated flight. The derived rate Ω_c serves as direct input for the rotational controller. In addition, the curve coordination compensates the centrifugal acceleration. Since the desired incremental motion required for the translation controller depends on the guidance, the estimation of $\delta\mathbf{u}_d$ is also done within the framework of the guidance controller ($\delta\mathbf{u}_d$-estimate). The overall architecture of this guidance is shown in Fig. 12.

4.2.1 Velocity and Position Control

The position and velocity controller are cascaded controllers, so the position controller determines a velocity command based on a position deviation. In contrast, the velocity controller determines a required virtual acceleration command to control the commanded velocity. The determined velocity and acceleration commands are obtained with an LQR approach. Assuming an ideal INDI transfer behavior, the transfer behavior of the translational INDI controller can be expressed using the transfer

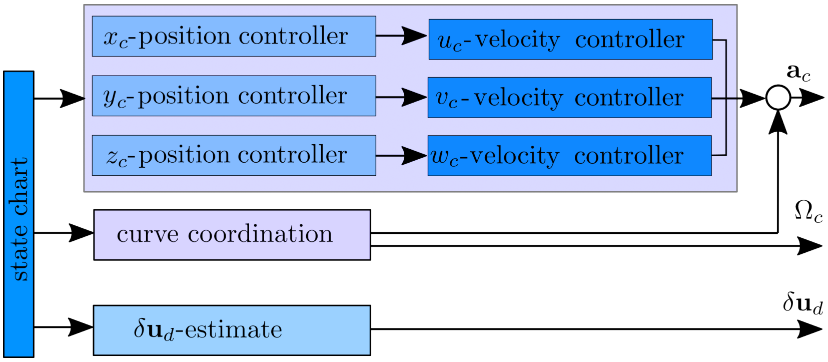

Figure 12. Architecture of the guidance controller.

behavior of the rotational controller and the propulsion units (see analysis of the transfer behavior for INDI in Smeur et al. (2016)). This allows the design of the LQR. The required transfer behavior from the acceleration to velocity and position can be determined by one or two additional integrations. Here, the cylindrical coordinate system is considered to calculate the deviation from the commanded position and velocity to the measured one. Accordingly, there are three decoupled velocities and two decoupled position controllers. It is, therefore, possible to specify a position in two axes and a velocity in the third. This way, the airborne system can be controlled on a circular path with a constant curve radius, height, and velocity by specifying an x_c-position, a z_c-position, and a v_c-velocity. The v_c-velocity command refers to the aerodynamic frame for the considered flight phases.

4.2.2 State chart

According to the flight regime, the guidance controller uses a look-up table presented in Tab. 1 to specify a transition height, a path radius, and an initial tether length for a measured wind field. Accordingly, the airborne system must be placed in the resulting VTOL zone, and the required tether length must be unwound. Starting above the VTOL zone at $\lambda_c = 90°$, the airborne system accelerates in an upwind direction with an active position controller in x_c- and z_c-direction and an active v_c-controller. The velocity command gradually increases to an airspeed of 16 m/s within this mode. According to the flight regime analysis, an acceleration of 1 $\mathrm{m/s^2}$ is aimed at. Once an airspeed of 12 m/s is reached, the roll transition begins until the airborne system is fully wing-borne. In order to increase the tether load, the position controller in y_c-direction is turned off, and only a u_c-command corresponding to $\dot{R}$ =0.2 m/s is set. This slowly increases the radius until the tether is stretched. Moreover, the mean elevation, which partially defines the orientation of the cylindrical coordinate system, can be changed to a value less than 90° to tilt the flight path. To reduce the tether force and return to a flight with a sagging tether, the position in y_c-direction is decreased by commanding the initial turning radius with a maximum radial velocity of $\dot{R}$ =-0.2 m/s. In order to exit the wing-borne flight state and begin the transition back to a prop-borne one, the airborne system has to yaw and build up a slip-angle, before a roll-transition back to a prop-borne flight can take place.

V_w, m/s	R_c, m	h_c, m	l_{tether}, m
2	40	30	52.5
4	40	40	59.4
6	60	40	75.7
8	60	50	82.0
10	60	50	82.0

Table 1. Look-up table for controllable operation of tailsitter AWES. The table lists recommended turn radius, transition height and tether length for different prevailing wind speeds (assume tether length ratio $k = 1.05$).

4.2.3 δu_d-estimate

Different desired motion commands are set for the translational controller depending on the state chart and the current flight state. For example, the longitudinal motion is defined by the pitch angle and mean throttle command in the prop-borne flight phases. However, the lateral motion is over-determined, allowing additional desired motion commands to be specified. In order to avoid strong airflow perpendicular to the wing surface, an incremental desired roll motion can be set. If the airflow hits the wing surface perpendicular, the airborne system must adjust its pitch attitude and deviate from a reference (no airflow perpendicular to the wing surface). The deviation of adjusted pitch attitude from this reference multiplied by a gain then results in the desired incremental roll motion ($\delta\phi_d$) aligning the airborne system wing plane with the direction of aerodynamic velocity. Considering a counterclockwise flight direction and an active roll-transition, this wing-alignment is deactivated, and a negative desired incremental roll angle is set. This ensures that the airborne system starts to roll until a wing-borne state is reached. In order to exit the wing-borne flight state and begin the transition back to a prop-borne one, a positive desired incremental roll angle and a negative incremental yaw angle ($\delta\phi_d$, $\delta\psi_d$) are set. This way, a slip angle can be built up, and the airborne system subsequently rolls back until a prop-borne flight state is reached again. δf_d and $\delta\theta_d$, i.e., the desired states for the thrust and the incremental pitch angle, are set to zero as the longitudinal motion is determined for all flight states. In the current implementation, $\delta\phi_d$, and $\delta\psi_d$ are limited by the maximum rotation rates to values of 30°/200 (controller frequency is set to 200 Hz). The ratio of the weights of controller deviation to these desired states is 10000. Current research is intensively concerned with the limits of the weights to ensure the INDI controller's stability with allocation.

4.2.4 Curve coordination

Within this block, the rate command Ω_c is computed to achieve a coordinated curve for a given turn radius and body velocity:

$$\Omega_c = \frac{V_{body}}{R} \tag{5}$$

Since the resulting virtual acceleration command from the velocity controller is based on the velocity deviations, the centrifugal acceleration from curved flight must also be considered. The compensation can be calculated as the cross product of the

405 measured and filtered ($_f$) body rates and velocity:

$$a_{comp} = \begin{bmatrix} p \\ q \\ r \end{bmatrix}_{b,f} \times \begin{bmatrix} u \\ v \\ w \end{bmatrix}_{b,f} \tag{6}$$

410 5 Simulation and Results

The control concept is tested for launching and landing in a model-in-the-loop simulation environment. The simulation is performed in MATLAB Simulink. The controller runs with a sampling time of 0.005s. In the following, a simulation for three different sections covering the phases of transition shown in Sec. 3.3 is presented and analyzed in detail. Similar to the cases analyzed in Fig. 9, a wind speed of 6 m/s is assumed. Following Tab. 1, the radius R_c is set to 60 m, and the transition height 415 h_c is set to 40 m. The simulation results for phase (i), including the curved yaw-roll transition, are in Fig. 13. As shown in the

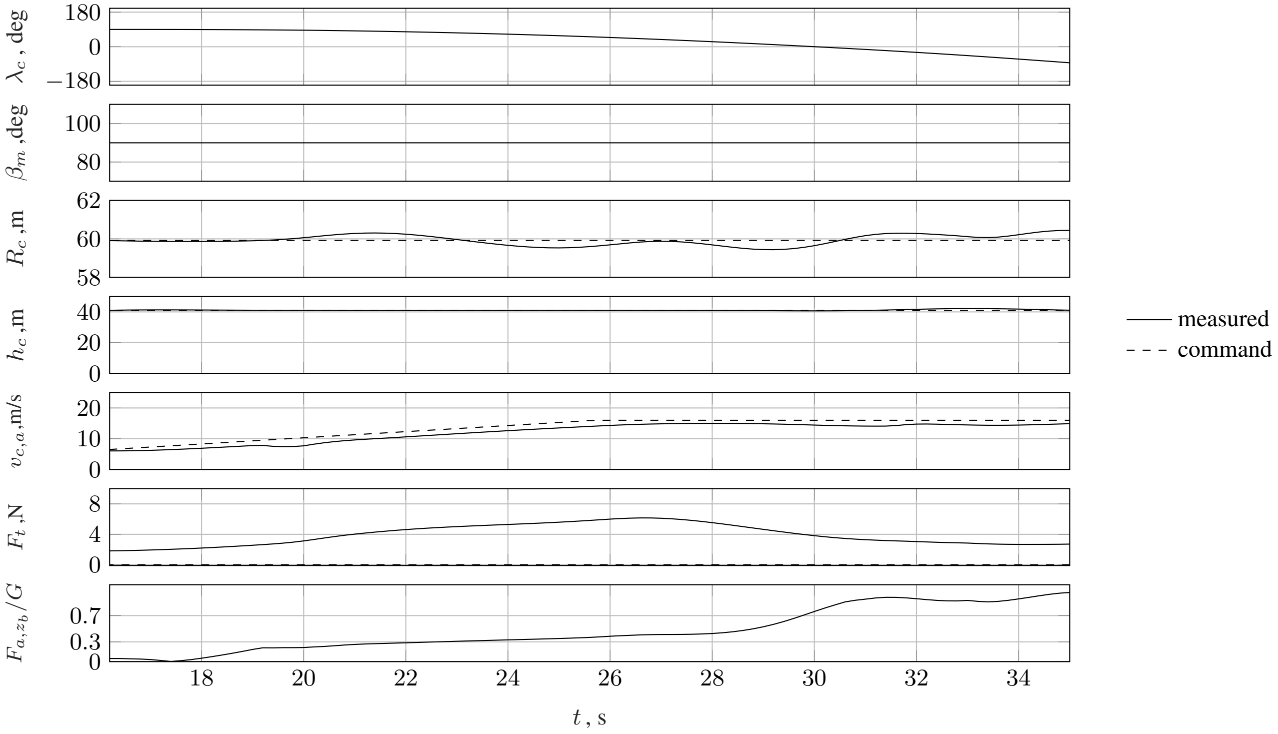

Figure 13. Simulation results for launching phase (i) (takeoff and acceleration along curved flight path, V_w=6 m/s, R_c=60 m, h_c=40 m).

velocity plot, the velocity command $v_{c,a}$ slowly increases, starting with 6 m/s (velocity of the prevailing wind field) and going up to 16 m/s. As soon as an aerodynamic velocity of 12 m/s is reached, the airborne system starts to roll, and the transition ratio ($F_{a,z_b}/G$) increases to about 1, indicating a fully wing-borne flight condition. During this transition, the radius and height remain constant. The small increase of the tether force during this phase can be explained by increasing aerodynamic loads 420 acting on the tether as it passes through an angular range of $0 < \lambda_c < 90°$. During this first phase, the mean elevation is kept constant at 90°. As indicated by a decrease in the mean elevation β_m from 90° to 80° in Fig. 14, the flight path tilts after 35 s. When the flight path is tilted, the height and radius deviate slightly more, but the deviation remains below 2 m. After a flight time of 60 s, the radius command is slowly increased until a threshold tether force of 12 N is measured and the controller switches to a tether force control mode. Here, the target force is set to 20 N. This force controller is not presented in the 425 previous section as it is not part of the actual transition control concept. It is used here to show that tethered flight can be achieved with this controller concept. As soon as the airborne system is supposed to transition back, the tether force controller is turned off, the radius and height controller activated, and the radius is reduced again to 60 m. As shown in Fig. 15, the flight path begins to tilt back to 90° at a flight time of about 110 s. When an average elevation of $\beta_m = 90°$ is reached, the transition back to the prop-borne flight state is initiated. For this purpose, the guidance controller commands a desired negative yaw and

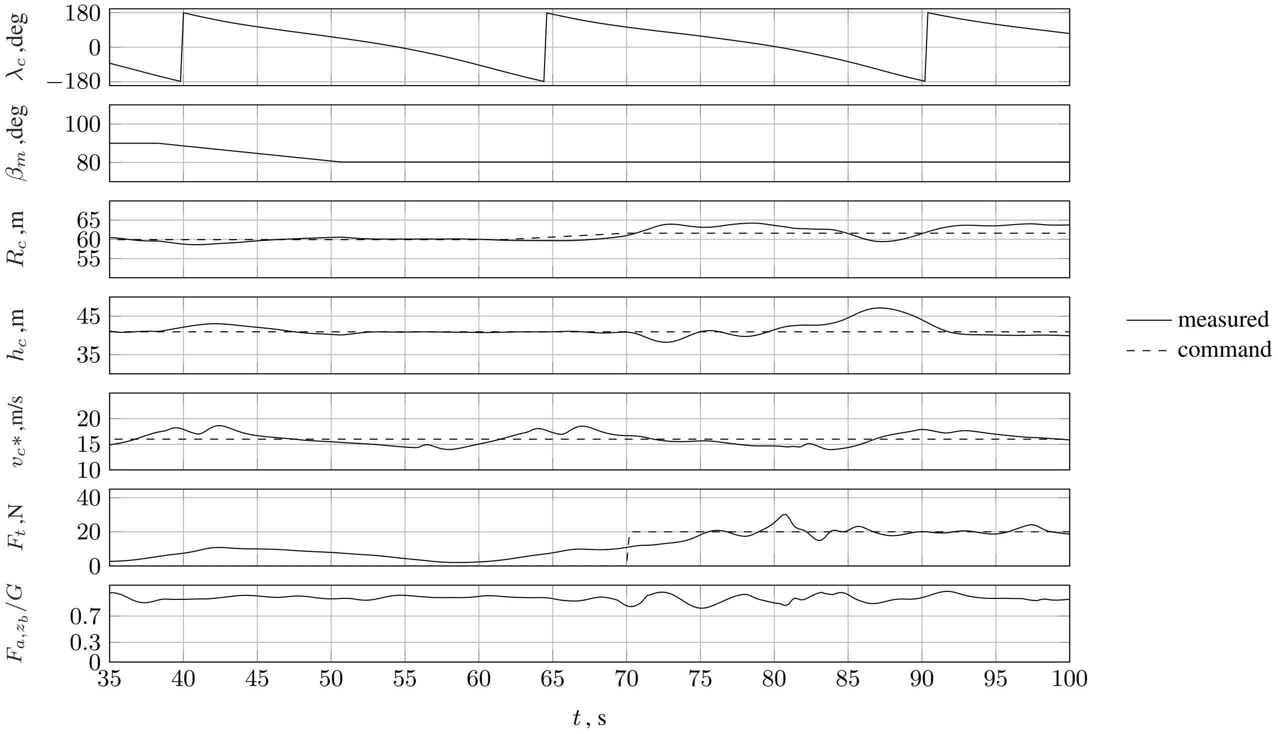

Figure 14. Simulation results for launching phase (ii) and tether force control phase (takeoff and acceleration along curved flight path, V_w=6 m/s, R_c=60 m, h_c=40 m).

430 positive roll motion while ensuring that the commanded radius, altitude, and velocity remain controlled. After approx. 140 s, the deceleration phase begins, and the airborne system decelerates with 1 m/s^2. The deceleration begins when the airborne system passes the power zone at $\lambda_c = 180°$. After approx. 155 s, the airborne system reaches the landing zone again and hovers back to the ground.

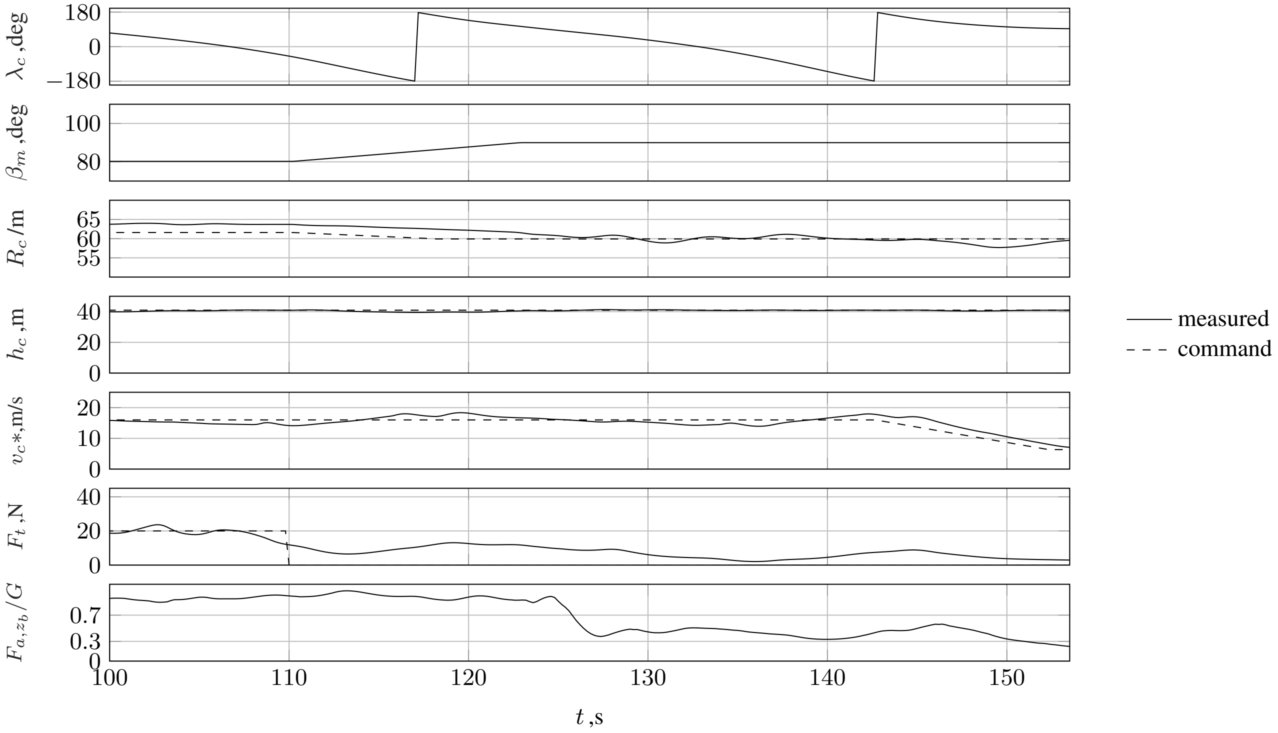

Figure 15. Simulation results for exit of tether force control phase and landing phase (decrease of radius, deceleration, begin of vertical flight back to the ground, V_w=6 m/s, R_c=60 m, h_c=40 m).

435 The simulation shows that the presented control concept achieves the desired results. The commanded radius and height can be controlled throughout the entire acceleration and transition from prop- to wing-borne with control deviations of less than 0.8 m. The tangential aerodynamic velocity is also controllable but deviates up to 3 m/s. This is due to the changing airspeed for a circular flight in a wind field. The flight phase from 70 s to 110 s shows that a tethered crosswind flight can be achieved and exited with the presented guidance concept. Similar to the transition from prop- to wing-borne, the transition from wing-borne 440 back to prop-borne can be achieved with position deviations of less than 2 m and a velocity deviation of less than 3 m/s.

6 Conclusions

This paper presents a control concept with a particular emphasis on the guidance of the launching and landing phases of a motorized flying wing AWES. First, the limitations associated with these two operational phases are examined to develop an appropriate guidance concept for this particular AWES. It is highlighted that the flight characteristics of such a VTOL-capable flying wing restrict its operation in vertical flight to a sagging tether with the wing aligned with the direction of airspeed. In light of these considerations, a guidance approach is presented whereby, for launching, an acceleration and multi-axial yaw-roll transition is performed on a curved path, followed by tether tensioning via roll motion. In order to facilitate a landing, the tether load is initially released, after which a roll-yaw transition and deceleration back to vertical prop-borne flight are performed. The advantage of this guidance approach is that it allows the tether force control to be kept with the airborne system, thus reducing the overall control complexity. In anticipation of future flight tests, this approach is also more practical, as the various stages of launching and landing can be tested step-wise. In light of the considerations above, an investigation into the controllability of this guidance is presented. The resulting flight regime demonstrates that the flight path radius and height are pivotal guidance parameters. As wind speed rises, the flight path radius and height must be increased to ensure the flying wing AWES remains controllable. Based on this, a flight controller has been developed which considers these constraints from the identified flight regime. The final section presents the results of a representative model-in-the-loop simulation with the presented guidance concept. The results demonstrate that the guidance concept implemented in the presented control structure successfully facilitates the desired launching and landing in simulations.

This work aims to establish a foundation for the guidance of a flying wing AWES, which will also facilitate the appropriate controller testing in field trials. Nevertheless, future research must identify alternative guidance concepts for launching and landing these special wind energy systems. The presented guidance concept defines the flight path by a strict set of parameters. Future research may focus on identifying additional arbitrary flight path shapes, which may deviate from inclined planar circles, to expand the flight regime. Furthermore, concerning the launching, this guidance approach can facilitate a more expeditious and seamless transition from vertical prop-borne flight to wing-borne flight and the gradual accumulation of the tether load. This may entail a combination of the pitch transition discussed and the yaw-roll transition. Similarly, the landing procedure aims to achieve a more rapid transition back to vertical prop-borne flight, which may also involve a combination of pitch transition and roll-yaw transition.

Author contributions. D. F. Duda is responsible for model development, overall implementation, and the paper. H. Fuest and D. F. Duda jointly developed the code to determine the trim points on a predefined grid of attitude angles. T. Islam and D. Moormann contributed to the conceptual design of the controller.

Competing interests. The contact author has declared that none of the authors has any competing interests.

Acknowledgements. Part of the research was performed within the EnerGlider (2018-2021) project. Special thanks are due to the Federal Ministry of Economic Affairs and Energy (BMWi) for the funding this project and to the Project Management Jülich for the support and coordination of the EnerGlider project.

https://doi.org/10.5194/wes-2024-90
Preprint. Discussion started: 20 August 2024

References

Ahrens, U., Diehl, M., and Schmehl, R.: Airborne Wind Energy -Book, ISBN 9783642399640, https://doi.org/10.1007/978-3-642-39965-7, 2013.

AWEurope: SkySails Group validates World's First Performance Curve for AWE, https://airbornewindeurope.org/aweurope-news/skysails-group-validates-worlds-first-performance-curve-for-airborne-wind-energy/, 2024.

Duda, D. F., Fuest, H., Islam, T., Ostermann, T., and Moormann, D.: Hybrid modeling approach for the tether of an airborne wind energy system, CEAS Aeronautical Journal, 13, 627–637, https://doi.org/10.1007/s13272-022-00581-7, 2022.

Eijkelhof, D. and Schmehl, R.: Six-degrees-of-freedom simulation model for future multi-megawatt airborne wind energy systems, Renewable Energy, 196, 137–150, https://doi.org/10.1016/j.renene.2022.06.094, 2022.

EnerKite GmbH: EnerKite GmbH-Web (accessed: 16.04.2024), https://enerkite.de/.

Fagiano, L., Zgraggen, A. U., Morari, M., and Khammash, M.: Automatic crosswind flight of tethered wings for airborne wind energy: Modeling, control design, and experimental results, IEEE Transactions on Control Systems Technology, 22, 1433–1447, https://doi.org/10.1109/TCST.2013.2279592, 2014.

Fuest, H., Duda, D. F., Islam, T., Ostermann, T., and Moormann, D.: Flight Control Architecture of a Rigid Flying Wing for Tethered Take-Off of an Airborne Wind Energy System, CEAS Aeronautical Journal, 12, 895–906, https://doi.org/10.1007/s13272-021-00545-3, 2021a.

Fuest, H., Duda, D. F., Islam, T., Ostermann, T., and Moormann, D.: Stabilization of the vertical take-off of a rigid flying wing for an airborne wind energy system, CEAS Aeronautical Journal, 12, 895–906, https://doi.org/10.1007/s13272-021-00545-3, 2021b.

Fuest, H., Duda, D. F., Islam, T., and Moormann, D.: Flight path and flight dynamic analysis of the starting procedure of a flying wing as airborne wind energy system, Deutscher Luft- und Raumfahrtkongress, Braunschweig Germany 2023, https://doi.org/10.21203/rs.3.rs-3847829/v1, 2023.

Hartmann, P.: Vorausschauende Flugbahnregelung für Kippflügelflugzeuge Predictive Flight Path Control for Tilt-Wing Aircraft, 2017.

Hochstenbach, M., Notteboom, C., Theys, B., and De Schutter, J.: Design and control of an unmanned aerial vehicle for autonomous parcel delivery with transition from vertical take-off to forward flight - VertiKUL, a quadcopter tailsitter, International Journal of Micro Air Vehicles, 7, 395–405, https://doi.org/10.1260/1756-8293.7.4.395, 2015.

Houle, C. and Luchsinger, R.: Demonstration of Energetic Potential, Safety and regulatory compliance of Airborne Wind Energy Systems in Switzerland on a pilot scale, www.bfe.admin.ch, 2021.

Jung, Y., Cho, S., and Shim, D. H.: A comprehensive flight control design and experiment of a tail-sitter UAV, in: AIAA Guidance, Navigation, and Control (GNC) Conference, p. 4992, ISBN 9781624102240, https://doi.org/10.2514/6.2013-4992, 2013.

KiteKRAFT GmbH: Kitekraft GmbH-Web (accessed: 29.07.2024), https://www.kitekraft.de/.

Kitemill: Kitemill-Web (accessed: 16.04.2024), https://www.kitemill.com/.

Li, B., Zhou, W., Sun, J., Wen, C. Y., and Chen, C. K.: Development of model predictive controller for a tail-sitter VTOL UAV in hover flight, Sensors (Switzerland), 18, 1–21, https://doi.org/10.3390/s18092859, 2018.

Liang, J., Fei, Q., Wang, B., and Geng, Q.: Tailsitter VTOL flying wing aircraft attitude control, Proceedings - 2016 31st Youth Academic Annual Conference of Chinese Association of Automation, YAC 2016, pp. 439–443, https://doi.org/10.1109/YAC.2016.7804934, 2017.

Loyd, M. L.: Crosswind Kite Power., Journal of energy, 4, 106–111, https://doi.org/10.2514/3.48021, 1980.

Makani Technologies LLC: Makani-Web (accessed: 29.07.2024), https://x.company/projects/makani/.

Makani Technologies LLC: Makani Technologies LLC-Web (accessed 31.07.2024), https://archive.org/details/makani-power, 2020a.

Makani Technologies LLC: Makani- The Energy Kite Report Part 1, Tech. rep., 2020b.

Martinez-Val, R.: Flying Wings. A New Paradigm for Civil Aviation?, Acta Polytechnica, 47, https://doi.org/10.14311/914, 2007.

Mozaero: Mozaero-Web (accessed: 08.08.2024), https://www.mozaero.com/.

Müller, J., Schatten, D., Duda, D. F., and Moormann, D.: Cascaded Indoor Flight Controller Design for a Miniaturized Tiltwing Aircraft, IMAV 2023: International Micro Air Vehicle Conference and Competition 2023, Aachen, Germany, September 11-15, 2023, 2023.

Rapp, S.: Robust Automatic Pumping Cycle Operation of AirborneWind Energy Systems, ISBN 9789055841745, https://doi.org/10.4233/uuid:ab2adf33-ef5d-413c-b403-2cfb4f9b6bae, 2019.

Rapp, S. and Schmehl, R.: Vertical takeoff and landing of flexible wing kite power systems, Journal of Guidance, Control, and Dynamics, 41, 2386–2400, https://doi.org/10.2514/1.G003535, 2018.

Ritz, R. and D'Andrea, R.: A global controller for flying wing tailsitter vehicles, Proceedings - IEEE International Conference on Robotics and Automation, pp. 2731–2738, https://doi.org/10.1109/ICRA.2017.7989318, 2017.

Sieberling, S.: Flight Guidance and Control of a Tethered Glider in an Airborne Wind Energy Application, Advances in Aerospace Guidance, Navigation and Control, pp. 337–351, 2013.

SkySails Power GmbH: SkySails power GmbH-(accessed 30.07.2024), https://skysails-power.com/.

Smeur, E. J., Chu, Q., and De Croon, G. C.: Adaptive incremental nonlinear dynamic inversion for attitude control of micro air vehicles, Journal of Guidance, Control, and Dynamics, 39, 450–461, https://doi.org/10.2514/1.G001490, 2016.

Smeur, E. J., Bronz, M., and de Croon, G. C.: Incremental control and guidance of hybrid aircraft applied to a tailsitter unmanned air vehicle, Journal of Guidance, Control, and Dynamics, 43, 274–287, https://doi.org/10.2514/1.G004520, 2020.

Stone, R. H., Anderson, P., Hutchison, C., Tsai, A., Gibbens, P., and Wong, K. C.: Flight testing of the T-wing tail-sitter unmanned air vehicle, Journal of Aircraft, 45, 673–685, https://doi.org/10.2514/1.32750, 2008.

Tal, E., Ryou, G., and Karaman, S.: Aerobatic Trajectory Generation for a VTOL Fixed-Wing Aircraft Using Differential Flatness, IEEE Transactions on Robotics, 39, 4805–4819, https://doi.org/10.1109/TRO.2023.3301312, 2023.

TwingTec: TwingTec-Web (accessed: 16.04.2024), https://twingtec.ch/.

Wang, X., Chen, Z., and Yuan, Z.: Modeling and control of an agile tail-sitter aircraft, Journal of the Franklin Institute, 352, 5437–5472, https://doi.org/10.1016/j.jfranklin.2015.09.012, 2015.

Williams, P.: Cable modeling approximations for rapid simulation, Journal of Guidance, Control, and Dynamics, 40, 1778–1787, https://doi.org/10.2514/1.G002354, 2017.

Wohlfahrt, K. and Nickel, M.: Schwanzlose flugzeuge : ihre auslegung und ihre eigenschaften, vol. 3, Springer-Verlag, ISBN 3-7643-2502-X, https://books.google.com/books?id=33fBLs7FhQ8C&lpg=PA577&dq=LippischHorten, 1990.